iScience

CellPress
OPEN ACCESS

Article

SARS-CoV-2 S1 protein causes brain inflammation by reducing intracerebral acetylcholine production

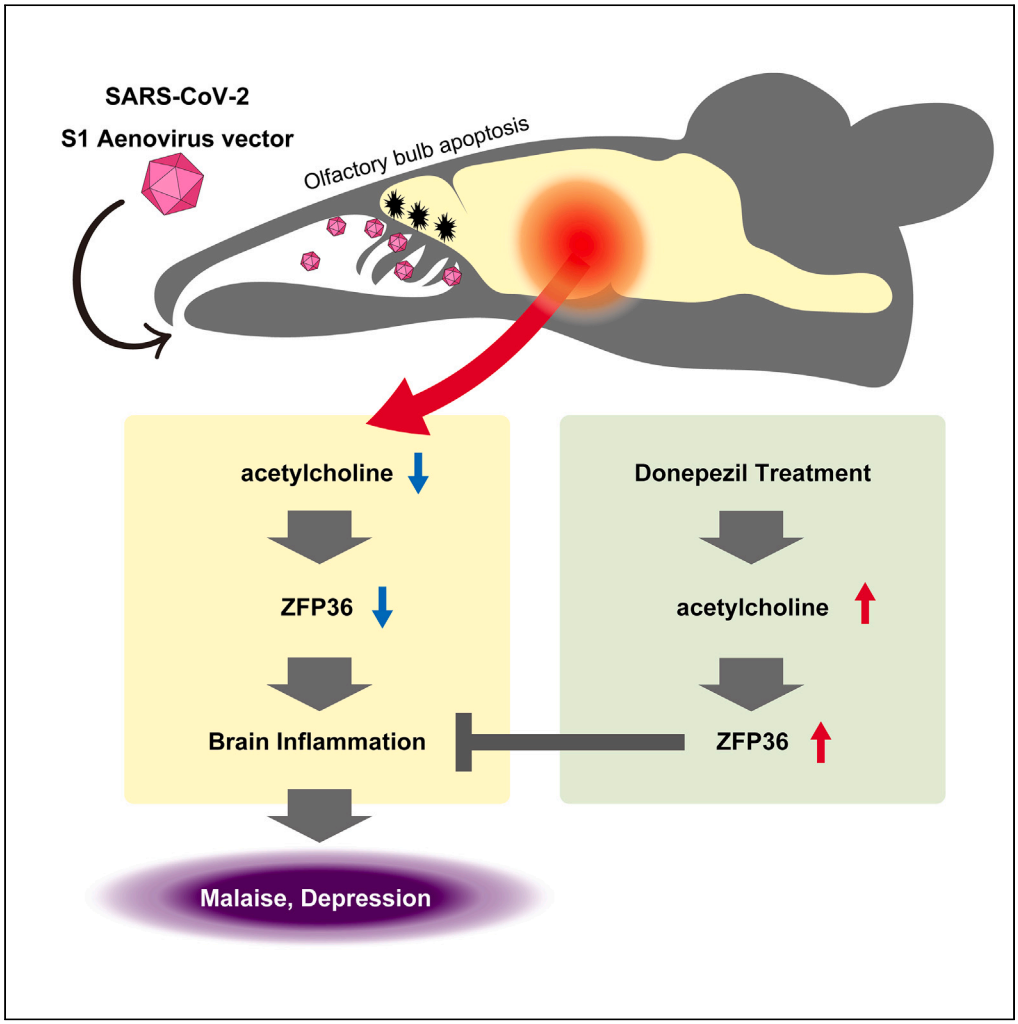

Naomi Oka, Kazuya Shimada, Azusa Ishii, Nobuyuki Kobayashi, Kazuhiro Kondo

kkondo@jikei.ac.jp

Highlights

Mice expressing S1 in the nasal cavity showed decreased acetylcholine production

In the brain, ZFP36 was decreased and inflammatory cytokine expression was enhanced

The mice exhibited malaise and depressive clinical signs

Donepezil normalized inflammatory cytokine production and mitigated depression

Oka et al., iScience 26, 106954
June 16, 2023 © 2023 The Author(s).
https://doi.org/10.1016/j.isci.2023.106954

iScience

CellPress
OPEN ACCESS

Article

SARS-CoV-2 S1 protein causes brain inflammation by reducing intracerebral acetylcholine production

Naomi Oka,[1] Kazuya Shimada,[1] Azusa Ishii,[1] Nobuyuki Kobayashi,[1] and Kazuhiro Kondo[1,2,*]

SUMMARY

Neurological complications that occur in SARS-CoV-2 infection, such as olfactory dysfunction, brain inflammation, malaise, and depressive symptoms, are thought to contribute to long COVID. However, in autopsies of patients who have died from COVID-19, there is normally no direct evidence that central nervous system damage is due to proliferation of SARS-CoV-2. For this reason, many aspects of the pathogenesis mechanisms of such symptoms remain unknown. Expressing SARS-CoV-2 S1 protein in the nasal cavity of mice was associated with increased apoptosis of the olfactory system and decreased intracerebral acetylcholine production. The decrease in acetylcholine production was associated with brain inflammation, malaise, depressive clinical signs, and decreased expression of the cytokine degrading factor ZFP36. Administering the cholinesterase inhibitor donepezil to the mice improved brain inflammation, malaise and depressive clinical signs. These findings could contribute to the elucidation of the pathogenesis mechanisms of neurological complications associated with COVID-19 and long COVID.

INTRODUCTION

Severe acute respiratory syndrome coronavirus 2 (SARS-CoV-2) is the causative virus of coronavirus disease 2019 (COVID-19). Mainly affecting the lungs, it causes pneumonia and acute respiratory distress syndrome (ARDS). Also affecting the kidneys, brain, heart, liver, and other organs, it can cause multi-organ failure.[1] Research on the etiology of SARS-CoV-2 has uncovered many neurological complications but many aspects of their pathogenesis mechanisms remain unknown.[2,3] Highly prevalent neurological complications are those due to olfactory system damage and brain inflammation, such as olfactory dysfunction, fatigue, and depressive symptoms.[4,5] If they persist, long COVID[6–8] may develop. Recently, long COVID has been listed in the ICD-10 classification as post-COVID-19 condition. The WHO defines post-COVID-19 condition "as the continuation or development of new symptoms 3 months after the initial SARS-CoV-2 infection, with these symptoms lasting for at least 2 months with no other explanation". Regarding symptoms, the WHO adds: "While common symptoms of long COVID can include fatigue, shortness of breath, and cognitive dysfunction over 200 different symptoms have been reported that can have an impact on everyday functioning".[9] Although several treatments have been established for COVID-19 and more are under development,[10–16] there is still no treatment for long COVID.[9,16–18]

Tissue damage in virus infection is normally due to proliferation of the virus in the tissue. In the autopsy results for patients who died from COVID-19, however, despite the presence of tissue degeneration in the brain, there was no evidence of CNS damage directly due to SARS-CoV-2 proliferation.[3,19–22] Also, since it has recently been reported that SARS-CoV-2 infection is not required for the onset of cognitive impairment in long COVID[23] and that there are few histopathologic changes[24] in patients with COVID-19 brain-related symptoms despite a substantial viral burden in their brains, many aspects of how SARS-CoV-2 causes such symptoms remain unknown. However, the point in common of these studies is that they suggest that factors other than the proliferation of the virus in the brain is at work.

Olfactory system cells are the first point of attack of SARS-CoV-2 and the plentiful expression of ACE2 and TMPRSS2, which is required for invasion of the virus,[25,26] makes it possible for SARS-CoV-2 to invade them. Olfactory bulb damage has indeed been reported in COVID-19 patients.[27–29]

[1]Department of Virology, The Jikei University School of Medicine, 3-25-8 Nishi-Shimbashi, Minato-ku, Tokyo 105-8461, Japan

[2]Lead contact

*Correspondence: kkondo@jikei.ac.jp

https://doi.org/10.1016/j.isci.2023.106954

This is an open access article under the CC BY-NC-ND license (http://creativecommons.org/licenses/by-nc-nd/4.0/).

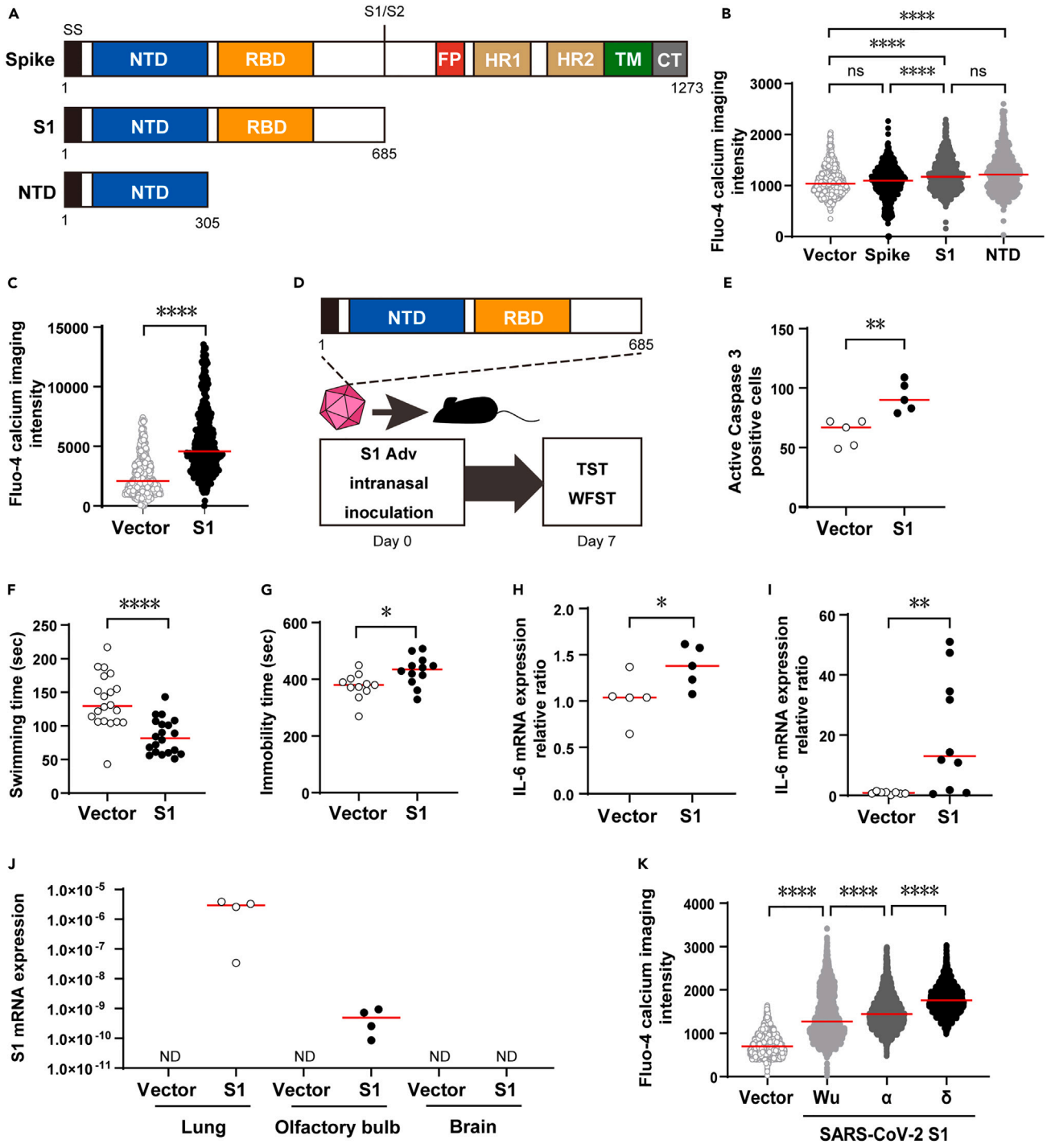

Figure 1. Analysis of spike protein function and creation of COVID-19 encephalopathy model using S1 protein

(A) Structures of genes used in expression experiments. SS, signal sequence; S1/S2, S1/S2 protease cleavage site; FP, fusion peptide; HR1, heptad repeat 1; R2, heptad repeat 2; TM, transmembrane domain; CT, cytoplasmic tail.

(B) Comparison of intracellular calcium concentration elevation among vector control, spike protein, S1 protein and NTD in mouse 3T3 cells. Calcium concentration was measured by fluorescence of Fluo-4. Vector control, n = 750; spike protein, n = 750; S1 protein, n = 746; NTD, n = 740; Kruskal-Wallis test followed by Dunn's post hoc test; median values; ****, $p < 0.0001$.

(C) Measurement of intracellular calcium concentration in human A549 cells. Calcium concentration was measured by fluorescence of Fluo-4. Vector control, n = 444; S1 Adv, n = 477; Mann-Whitney U-test; median values; ****, $p < 0.0001$.

(D) S1 mouse creation and evaluation.

Figure 1. *Continued*

(E) Measurement of apoptosis induction in S1 mouse olfactory bulb tissue based on caspase 3 positive cell count (vector control, n = 5; S1 mouse, n = 5; Mann-Whitney U-test; median values; **, $p < 0.01$).

(F) Reduced swimming time in S1 mouse WFST; i.e., increase in fatigue (vector control, n = 20; S1 mouse, n = 20; Mann-Whitney U-test; median values; ****, $p < 0.0001$).

(G) Prolonged immobility time in S1 mouse TST, i.e., increase in depressive clinical signs (vector control, n = 11; S1 mouse, n = 12; Mann-Whitney U-test; median values; *, $p < 0.05$).

(H) Enhanced IL-6 expression in S1 mouse brain tissue (vector control, n = 5; S1 mouse, n = 5; Mann-Whitney U-test; median values; *, $p < 0.05$).

(I) Enhanced IL-6 expression in S1 mouse lung tissue (vector control, n = 10; S1 mouse, n = 10; Mann-Whitney U-test; median values; **, $p < 0.01$).

(J) S1 mRNA expression in lung, olfactory bulb and brain tissue (Ratios of S1 to 18s ribosomal RNA are shown.) (vector control, n = 4 each; S1 mouse, n = 4 each median values).

(K) Comparison of intracellular calcium concentration elevation among Wu strain, α strain, and δ strain in mouse 3T3 cells. Calcium concentration was measured by fluorescence of Fluo-4. Vector control, n = 3562; Wu strain, n = 2711; α strain, n = 2837; δ strain, n = 2339; Kruskal-Wallis test followed by Dunn's post hoc test; median values; ****, $p < 0.0001$.

Furthermore, since it was reported that surgically induced disruption of olfactory bulb function by olfactory bulbectomy (OBX) resulted in brain inflammation,[30–32] we considered that olfactory bulb damage due to SARS-CoV-2 was related in some way to the onset of brain inflammation.

It has been reported that the olfactory system cell damage, in particular that in the olfactory bulb, results from an increase in intracellular calcium in olfactory epithelial cells.[33] In previous research, we demonstrated that production of the human herpesvirus-6 (HHV-6) protein SITH-1, which has calcium elevating activity in olfactory cells, induced apoptosis in the olfactory bulb and caused depression.[34] Since, SARS-CoV-2 spike protein is also known to elevate calcium in cells,[35] we created a mouse model expressing spike protein in the nasal cavity.

RESULTS

Intracellular calcium elevating activity of S1 protein

When spike protein invades cells, it is cleaved into S1 and S2 subunits. Using mouse cells (3T3), we found that the N-terminal domain (NTD) was responsible for calcium elevating activity on S1 protein (Figures 1A and 1B). S1 protein also elevated intracellular calcium in human cells (A549) (Figure 1C).

Therefore, in order to investigate the effect of S1 protein's intracellular calcium elevating activity on the olfactory bulb *in vivo*, we induced expression of S1 protein in the mouse olfactory cavity. In brief, we prepared a non-proliferative adenovirus vector (S1 Adv) expressing the S1 protein of the original Wuhan strain (Wu strain) and then created the S1 mouse through inoculation of S1 Adv into the nasal cavity. One week after inoculation, we conducted behavioral experiments and observed gene expression (Figure 1D).

S1 expressing mouse manifests olfactory bulb damage, malaise, depression, and brain inflammation

Apoptosis of the olfactory bulb was enhanced in the model mouse expressing S1 protein in the nasal cavity (S1 mouse) as expected (Figure 1E). Since it was reported that surgically induced disruption of olfactory bulb function by olfactory bulbectomy (OBX) resulted in depressive-like clinical signs[36] and brain inflammation,[31] we conducted depression- and malaise-related behavioral tests, and brain inflammation-related investigations. Owing to a decrease in swimming time in the weight-loaded forced swim test (WFST),[37] we determined that fatigue had increased in the S1 mouse (Figure 1F). In addition, there was an increase in immobility time for the S1 mouse in the tail suspension test (TST)[38] (Figure 1G), which we interpreted as presence of depressive clinical signs.

In addition, using histologic samples of the whole brain without the olfactory bulb, we observed enhanced expression of inflammatory cytokines (IL-6, TNFα) and a chemokine (CCL-2) with an inflammation promoting function (Figures 1H, S1A, and S1B) suggesting that inflammation had occurred in the brain.

We also observed enhanced expression of IL-6 in the lungs (Figure 1I). In the lungs, a correlation of inflammatory cytokine production with S1 mRNA expression (Figures S1C and S1D) suggested that inflammation in the lungs was due to the inflammation-inducing action of S1 protein.[39] In contrast, since S1 mRNA expression was not detected in the brain, this suggested that inflammation in the brain was due to an indirect effect (Figure 1J).

Since the results up to this point had suggested an association of S1 protein's calcium increasing activity and pathogenicity, we measured this for S1 protein from the Wu strain, α strain, and δ strain. The strength of intracellular calcium concentration elevation activity in cells expressing the different strains was in the order: Wu < α < δ (Figure 1K). This was consistent with the order for the severity and mortality rates of these strains: Wu < α < δ.[40,41]

Impairment of acetylcholine's anti-inflammatory effect was associated with brain inflammation in S1 mouse

To elucidate a mechanism for the effect of olfactory bulb damage on the brain and the body overall, we focused on neurotransmitters in neurons connecting to the olfactory bulb. There was a decrease in cells positive for the acetylcholine synthesizing enzyme choline acetyltransferase (ChAT) in the medial septal (MS) and diagonal band of Broca (DBB) (Figures 2A and 2B) and the acetylcholine level in the brain overall was also decreased (Figure 2C). We therefore examined a relationship between brain inflammation in the S1 mouse and the anti-inflammatory response in which acetylcholine plays a role called cholinergic anti-inflammatory pathway (CAP).[42] CAP was discovered as a mechanism for suppressing inflammation in peripheral tissues via autonomic nerve fibers. It is also known to have a function for suppressing inflammation in the brain.[43,44] Since an α7 nicotinic acetylcholine receptor (α7nAchR) agonist was found to activate CAP,[44] one week after inoculation with S1 Adv, we administered the α7nAchR agonist PNU282987 intracerebroventricularly (i.c.v.) and after an hour, measured inflammatory cytokine expression levels in the brain (Figure 2D). This resulted in normalizing the enhanced inflammatory cytokine expression in the S1 mouse (Figure 2E). These observations suggest that brain inflammation in the S1 mouse resulted from CAP disruption.

It has been known for some time that nerves in the CAP suppress inflammation,[42,45] but inflammation suppressing factors were unknown. In the S1 mouse, the expression of the mRNA binding protein ZFP36,[46] which has an inflammatory cytokine mRNA degrading function, was reduced when inflammation was present in the brain and was increased by PNU282987 (Figure 2F). In contrast, with another RNA binding protein having an inflammatory cytokine mRNA degrading function similar to that of ZFP36, expression was not decreased, and not induced by PNU282987 in the S1 mouse brain (Figure S2). Also, administering PNU282987 to the human astrocyte cell line U373[47] expressing α7nAchR enhanced ZFP36 expression and suppressed TNFα expression (Figures 2G and 2H). These findings suggest that ZFP36 functions as an inflammation-suppressing factor in the CAP.

In order to investigate the influence of systemic inflammation in brain inflammation, we administered lipopolysaccharide (LPS) intraperitoneally to the S1 mouse to enhance systemic inflammation and investigated expression of neural differentiation markers in the olfactory bulb and brain. As a result, the expression of calbindin,[48,49] a GABAergic neuron marker, was markedly decreased. (Figures 2I and 2J). As no changes were observed in other neuron differentiation markers (Figures S3A and S3B), this observation was considered specific to GABAergic neurons.

Acetylcholine esterase inhibitor donepezil improves brain symptoms

The acetylcholine esterase inhibitor donepezil is a central cholinergic agent used clinically for the treatment of dementia.[50] To investigate the possibility of its repurposing for the treatment of neurological complications in COVID-19, we investigated symptom improvement due to donepezil in the S1 mouse.

We administered donepezil at the usual dose for animal experiments (4 mg/kg/day) from the day of S1 Adv inoculation daily in drinking water (Figure 3A). Administration of donepezil resulted in normalizing inflammatory cytokines (IL-6, TNFα) that had been enhanced by S1 protein (Figures 3B and S4A). Since IL-6 and TNFα genes are targets of ZFP36,[46,51] this finding suggests that donepezil brought about a recovery in CAP. However, administration of donepezil did not mitigate the enhanced inflammatory cytokine production in the lungs (Figures S4B–S4D).

Regarding pathological changes in the brain, donepezil mitigated the enhanced apoptosis in the olfactory bulb of the S1 mouse (Figures 3C and 3D). There was also improvement due to donepezil with regard to doublecortin (DCX) positive cells, which indicate hippocampal neurogenesis and had been decreased in the S1 mouse (Figures 3E and 3F). A decrease in hippocampal neurogenesis has been reported to be associated with depressive symptoms[52] and memory impairment,[53] so we considered it likely that donepezil would

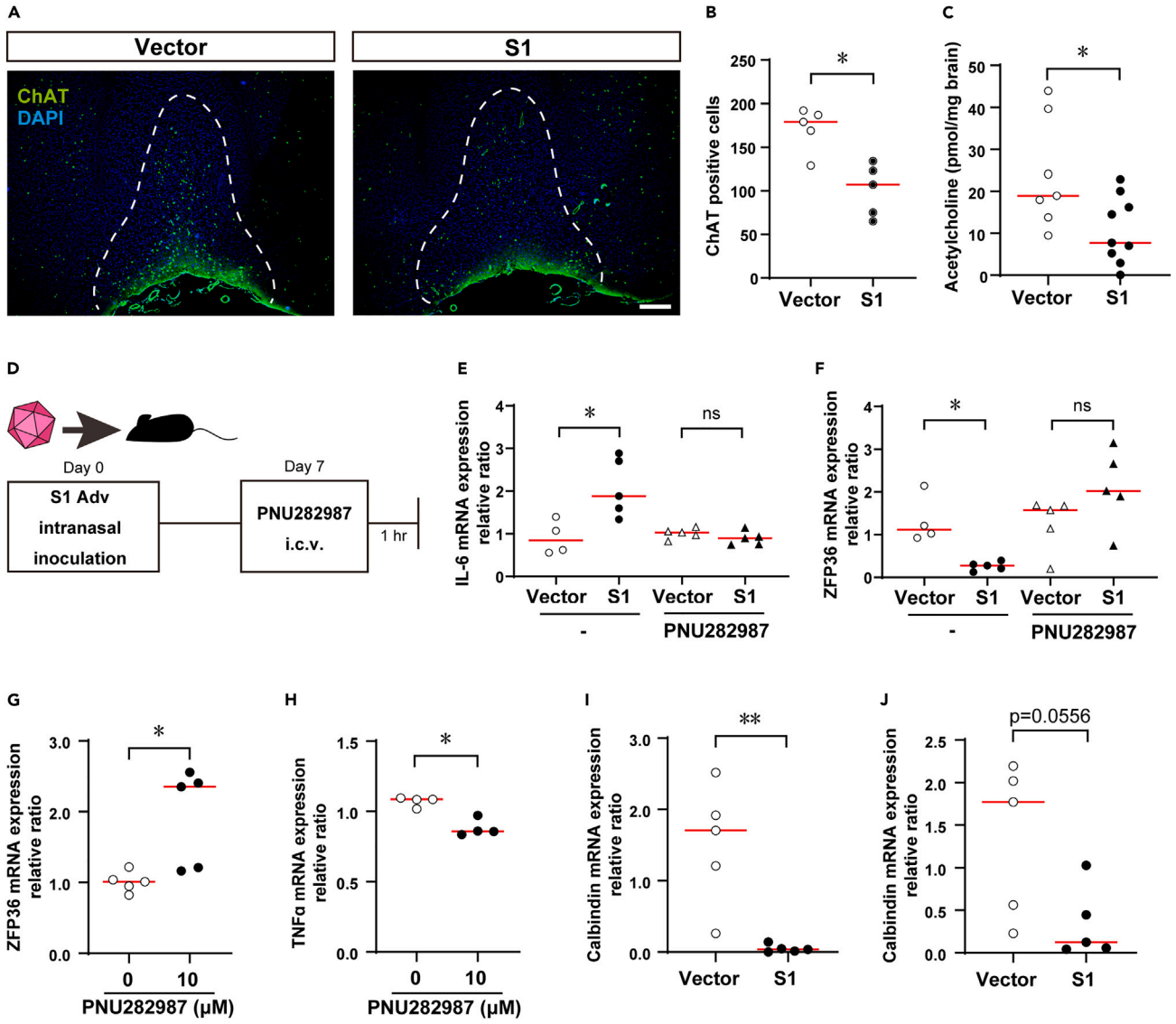

Figure 2. Disruption of cholinergic anti-inflammatory pathway (CAP) in S1 mouse brain

(A) Decreased ChAT positive cells in S1 mouse MS and DBB (green, ChAT; blue, DAPI; scale bar, 200 μm).

(B) Decreased ChAT positive cells in S1 mouse MS and DBB (vector control, n = 5 S1 mouse, n = 5; Mann-Whitney U-test; median values; *, $p < 0.05$).

(C) Intracerebral acetylcholine (vector control, n = 8; S1 mouse, n = 9; Mann-Whitney U-test; median values; *, $p < 0.05$).

(D) Adv inoculation, PNU282987 administration, brain harvest schedule.

(E) Enhanced IL-6 expression in S1 mouse brain tissue and effect of PNU282987 (no treatment; vector control, n = 4 S1 mouse, n = 5; Mann-Whitney U-test; median values; *, $p < 0.05$. PNU282987; vector control, n = 5 S1 mouse, n = 5; Mann-Whitney U-test; median values; ns, not significant.).

(F) Decreased ZFP36 expression in S1 mouse brain tissue and effect of PNU282987 (no treatment; vector control, n = 4 S1 mouse, n = 5; Mann-Whitney U-test; median values; *, $p < 0.05$. PNU282987; vector control, n = 5 S1 mouse, n = 5; Mann-Whitney U-test; median values; ns, not significant.).

(G) ZFP36 mRNA expression in U373 cells (LPS stimulation, n = 5; LPS stimulation+PNU282987 treatment, n = 5; Mann-Whitney U-test; median values; *, $p < 0.05$).

(H) TNFα mRNA expression in U373 cells (LPS Stimulation, n = 5; LPS stimulation+PNU282987 treatment, n = 5; Mann-Whitney U-test; median values; *, $p < 0.05$).

(I) Expression of calbindin in olfactory bulb tissue of S1 mice additionally administered LPS (vector control, n = 5 S1 mouse, n = 5; Mann-Whitney U-test; median values; **, $p < 0.01$).

(J) Expression of calbindin in brain tissue of S1 mouse additionally administered LPS (vector control, n = 4 S1 mouse, n = 5; Mann-Whitney U-test; median values).

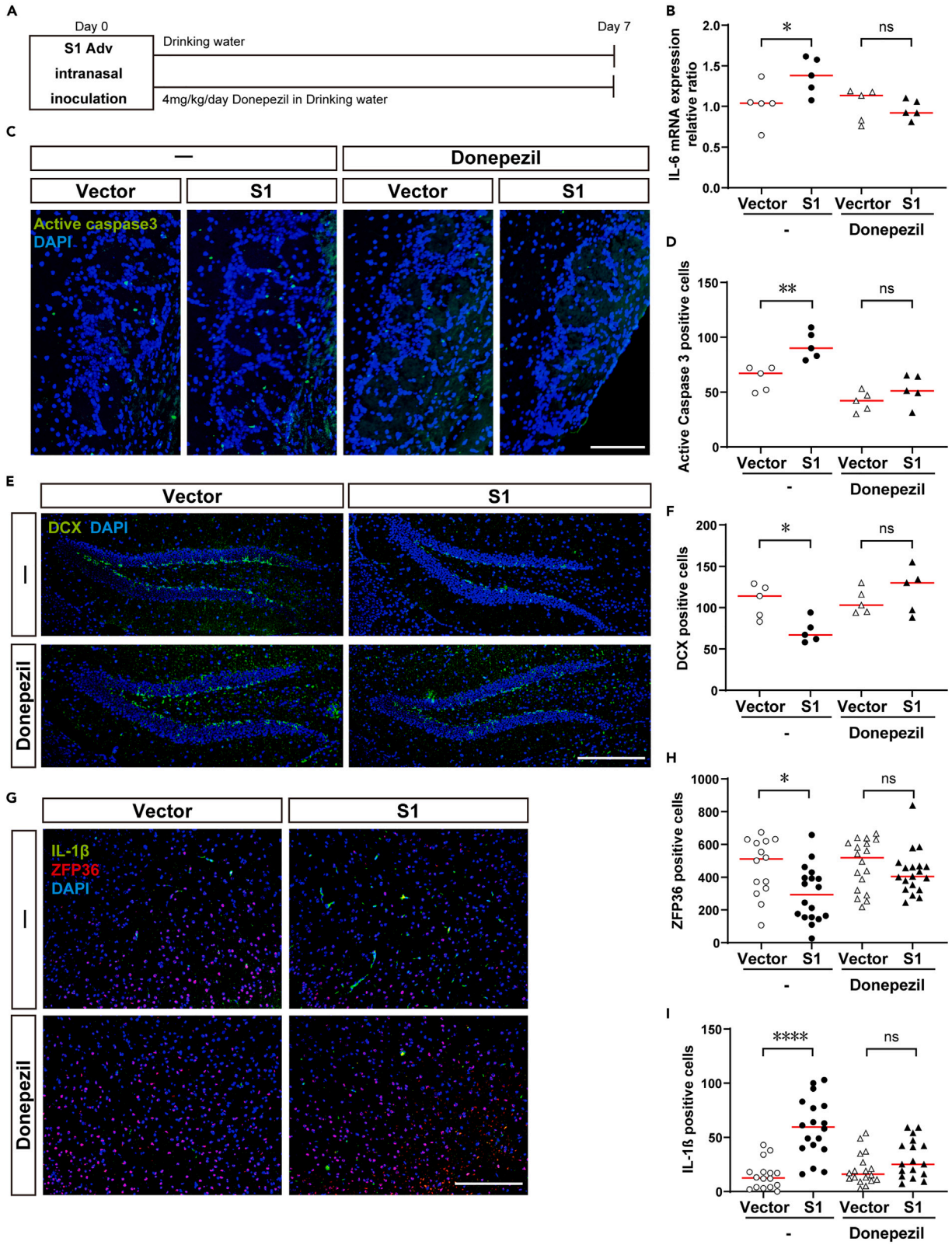
A
Day 0
S1 Adv
intranasal
inoculation
Drinking water
Day 7
4mg/kg/day Donepezil in Drinking water
B
IL-6 mRNA expression relative ratio
2.0
1.5
1.0
0.5
0.0
*
ns
Vector
S1
Vecrtor
S1
-
Donepezil
C
—
Donepezil
Vector
S1
Vector
S1
Active caspase3
DAPI
D
Active Caspase 3 positive cells
150
100
50
0
**
ns
Vector
S1
Vector
S1
-
Donepezil
E
Vector
S1
—
Donepezil
DCX DAPI
F
DCX positive cells
200
150
100
50
0
*
ns
Vector
S1
Vector
S1
-
Donepezil
G
Vector
S1
—
Donepezil
IL-1β
ZFP36
DAPI
H
ZFP36 positive cells
1000
800
600
400
200
0
*
ns
Vector
S1
Vector
S1
-
Donepezil
I
IL-1ß positive cells
150
100
50
0
****
ns
Vector
S1
Vector
S1
-
Donepezil

Figure 3. Mitigation of olfactory and brain dysfunction in S1 mouse due to donepezil

(A) Adv inoculation, donepezil administration, brain harvest schedules.

(B) Enhanced IL-6 expression in S1 mouse brain tissue and improvement due to donepezil (no treatment; vector control, n = 4, S1 mouse, n = 5; Mann-Whitney U-test; median values; *, $p < 0.05$. Donepezil; vector control, n = 5, S1 mouse, n = 5; Mann-Whitney U-test; median values; ns, not significant).

(C) Increased apoptosis cells in olfactory bulb tissue of S1 mouse and improvement due to donepezil (green, Active caspase 3; blue, DAPI; scale bar, 100 μm).

(D) Increased caspase 3 positive apoptotic cells in S1 mouse olfactory bulb tissue and improvement due to donepezil (no treatment; vector control, n = 5, S1 mouse, n = 5; Mann-Whitney U-test; median values; **, $p < 0.01$. Donepezil; vector control, n = 5 S1 mouse, n = 5; Mann-Whitney U-test; median values; ns, not significant).

(E) Decreased DCX positive cells in S1 mouse hippocampus tissue and improvement due to donepezil (green, DCX; blue, DAPI; scale bar, 200 μm).

(F) Decreased DCX positive cells in S1 mouse hippocampus tissue and improvement due to donepezil (no treatment; vector control, n = 5, S1 mouse, n = 5; Mann-Whitney U-test; median values; *, $p < 0.05$. Donepezil; vector control, n = 5 S1 mouse, n = 5; Mann-Whitney U-test; median values; ns, not significant.).

(G) Increased IL-1β positive cells in S1 mouse amygdala tissue and improvement due to donepezil (green, IL-1β; red, ZFP36; blue, DAPI; scale bar, 200 μm).

(H) Decreased ZFP36 positive cells in S1 mouse amygdala tissue and improvement due to donepezil (no treatment; vector control, n = 14, S1 mouse, n = 18; Mann-Whitney U-test; median values; *, $p < 0.05$. Donepezil; vector control, n = 18 S1 mouse, n = 19; Mann-Whitney U-test; median values; ns, not significant.).

(I) Increased IL-1β positive cells in S1 mouse amygdala tissue and improvement due to donepezil (no treatment; vector control, n = 16, S1 mouse, n = 18; Mann-Whitney U-test; median values; ****, $p < 0.0001$. Donepezil; vector control, n = 18 S1 mouse, n = 17; Mann-Whitney U-test; median values; ns, not significant.).

improve depressive symptoms and memory impairment in COVID-19. However, donepezil did not reverse a decrease in ChAT positive cells in the MS and DBB (Figures S4E and S4F).

Using anti-ZFP 36 antibody and anti-IL-1β antibody available for use in immunohistochemistry, we performed histologic staining of sections of brain tissue sections innervated with cholinergic nerves from the MS and DBB. For the amygdala, we obtained distinct staining images of decreased ZFP36 production and enhanced IL-1β production due to administration of S1. These phenomena were canceled by administering donepezil (Figures 3G–3I).

Treatment of neurological complications in COVID-19 with donepezil

With the objective of using donepezil clinically to treat neurological complications in COVID-19 in mind, we examined the drug's effects on clinical signs, as well as the dose that would be effective.

We administered donepezil at the usual dose for animal experiments (4 mg/kg/day) daily in drinking water from the day of S1 Adv inoculation (Figure 4A). The administration of donepezil mitigated the increased fatigue determined in the weigh-loaded swimming test and depressive clinical signs determined from the TST (Figures 4B and 4C).

Next, we investigated whether the normal dose of donepezil used for dementia would be effective. We converted the normally administered dose for dementia patients (5 mg/day) for mice (1 mg/kg/day) and administered a single dose orally. Administration was one week after inoculation of S1 Adv and measurements were made 2 h later (Figure 4D). A tendency toward mitigation of the enhanced expression of inflammatory cytokines (IL-6, TNFα) and a chemokine (CCL-2) was observed in the S1 mouse brain (Figures 4E–4G). This result indicates the possibility of donepezil being effective against brain inflammation in COVID-19 at the normal dose.

DISCUSSION

SARS-CoV-2 S1 protein has calcium elevating activity. By inducing its expression in the mouse nasal cavity, we created an S1 mouse exhibiting neurological complications, such as olfactory bulb damage, brain inflammation, fatigue, and depressive clinical signs. This was consistent with brain inflammation induced by olfactory bulb damage that was reported for OBX, as well as induction of depressive clinical signs due to expression in olfactory epithelium of HHV-6 SITH-1 protein, which also has calcium elevating activity. In addition, it has been reported that olfactory system cell damage due to calcium elevation is due to microangiopathy[33] and this is consistent with autopsy results for COVID-19 patients.[54]

In addition, a lack of S1 mRNA expression in the brain led us to conclude that we had reproduced a state of encephalopathy similar to that reported for COVID-19, where the inflammation is not due to viral proliferation in the brain but caused indirectly.

The finding that strength of calcium elevating activity for different strains was in the order $Wu < \alpha < \delta$ is of great interest because this is consistent with the order of their severity and mortality rates.[40,41] Regarding

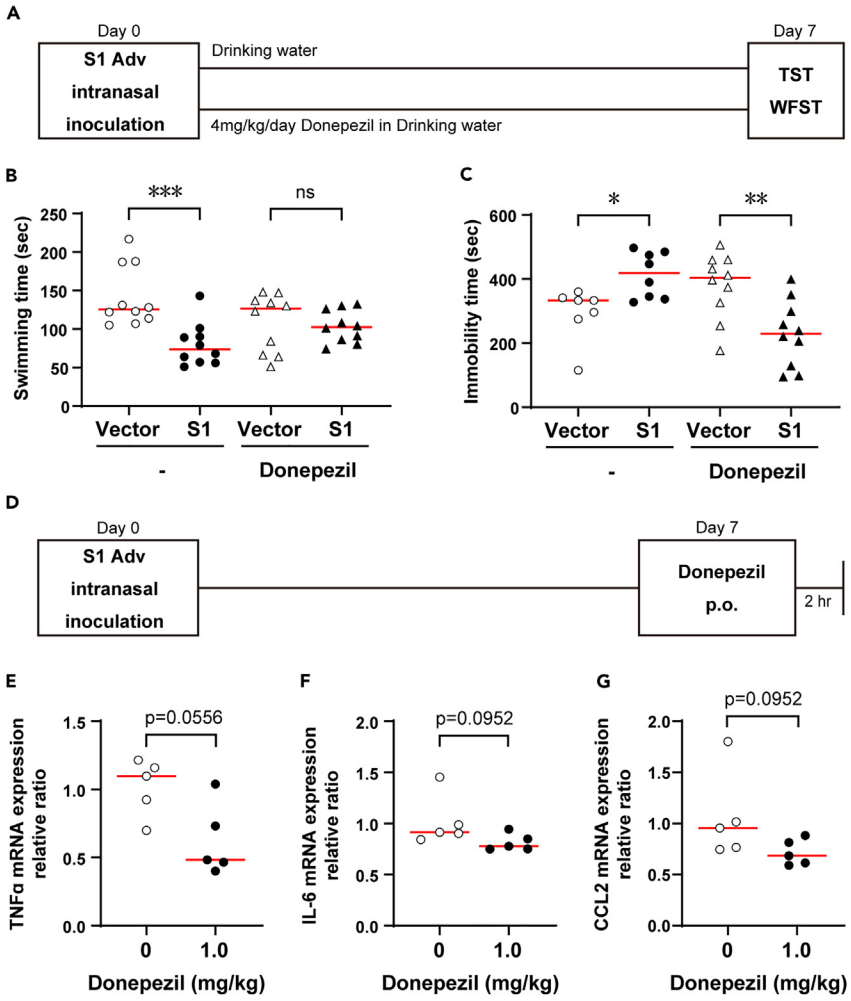

Figure 4. Therapeutic effects of donepezil with respect to COVID-19

(A) Adv inoculation, donepezil administration, behavior experiment schedules.

(B) Decreased S1 mouse swimming time in WFST, i.e., increase in fatigue, and therapeutic effect of donepezil (no treatment; vector control, n = 10, S1 mouse, n = 10; Mann-Whitney U-test; median values; ***, $p < 0.001$. Donepezil; vector control, n = 10 S1 mouse, n = 10; Mann-Whitney U-test; median values; ns, not significant).

(C) Increased immobility time in S1 mouse TST and therapeutic effect of donepezil (no treatment; vector control, n = 7, S1 mouse, n = 8; Mann-Whitney U-test; median values; *, $p < 0.05$. Donepezil; vector control, n = 10 S1 mouse, n = 10; Mann-Whitney U-test; median values; ns, not significant).

(D) Adv inoculation, donepezil administration, organ harvest schedules.

(E) Inhibitory effect of donepezil on TNFα expression in S1 mouse brain tissue (0 mg/kg, n = 5; 1 mg/kg, n = 5; Mann-Whitney U-test; median values).

(F) Inhibitory effect of donepezil on IL-6 expression in S1 mouse brain tissue (0 mg/kg, n = 5; 1 mg/kg, n = 5; Mann-Whitney U-test; median values).

(G) Inhibitory effect of donepezil on CCL2 expression in S1 mouse brain tissue (0 mg/kg, n = 5; 1 mg/kg, n = 5; Mann-Whitney U-test; median values).

the calcium-related pathogenicity of spike protein and SARS-CoV-2, an association with syncytia formation has been found.[35] The mechanism indicated in the present study may also make consistency between strength of calcium enhancing activity and pathogenicity easier to explain.

In the brain of the S1 mouse, we observed a decrease in cells positive for ChAT in the MS and DBB, as well as a decrease in the amount of acetylcholine in the brain and CAP disruption.[42,45] We considered neurological complications had developed in the S1 mouse because inflammation in the brain caused by inflammatory cytokines produced in the lungs could not be suppressed due to CAP disruption. Since it was reported that

COVID-19 symptoms were mitigated by nicotine administered through smoking, much attention has been given to a relationship between COVID-19 and CAP.[55,56] Decreased expression of acetylcholine receptors in the peripheral blood of COVID-19 patients has also been reported.[57]

Since it was reported that surgically induced disruption of olfactory bulb function by OBX resulted in a decrease in ChAT positive cells in the MS,[58] the decrease in ChAT positive cells and disruption of the CAP in the S1 mouse could be due to olfactory bulb dysfunction. Thus, severe damage to the olfactory bulb due to SARS-CoV-2 infecting the olfactory system[27,54] could be the main cause of CAP disruption in COVID-19. However, the olfactory bulb damage in the S1 mouse was thought to be due to the calcium elevating activity of S1 protein.

Our results thus far suggest that, in the S1 mouse, inflammatory cytokines produced in the lungs due to S1 protein expression induce inflammation in the brain because anti-inflammatory effects are diminished due to CAP impairment. Systemic inflammation due to proliferation of the virus throughout the body in COVID-19 could be stronger than that in observed in the S1 mouse. Therefore, we enhanced systemic inflammation through intraperitoneal administration of lipopolysaccharide (LPS), which resulted in markedly reduced expression of the GABAergic marker calbindin[59] in the olfactory bulb and the brain. The olfactory bulb has many GABAergic neurons,[60] and it has been reported that GABAergic dysfunction is the cause of cognitive difficulties in long COVID.[61,62] Thus, our finding may help explain the pathogenesis mechanism of olfactory disturbance and brain fog in long COVID.

To mitigate the pathological state in the S1 mouse, we administered donepezil for inhibition of choline esterase, the enzyme that breaks down acetylcholine. This resulted in reversing the inflammation, reduced hippocampal neurogenesis and apoptosis in the olfactory bulb, and the fatigue and depressive clinical signs associated with them also disappeared.

In the histologic examination of the S1 mouse brain, decreased ZFP36 production, enhanced inflammatory cytokine (IL-1β) production as well as their mitigation by donepezil was more distinct in the amygdala than other parts. This suggests that the amygdala was the most strongly affected by enhancement of inflammation due to CAP disruption in the S1 mouse. It has been reported that the changes in gene expression,[63] metabolic function, and[64] vol[65] indeed occur in the amygdala of COVID-19 patients. In addition, damage to the amygdala has been found to be associated with long COVID[64,66,67] Therefore, the information that we obtained regarding inflammation in the amygdala of the S1 mouse and its mitigation by donepezil may be useful in research on long COVID.

As donepezil readily passes through the blood-brain barrier (BBB) and has a brain to blood drug concentration ratio of 4 or above,[68] we considered that these improvements were due to the action of donepezil acting in the brain.

On the other hand, the decrease in ChAT positive cells in the MS and DBB was not reversed by donepezil. This finding again suggests that a decrease in ChAT positive cells is positioned upstream of a series of pathological states and is considered to provide a basis for an increase in acetylcholine due to donepezil having a therapeutic effect on the overall clinical signs in the S1 mouse.

Our findings indicate that administering donepezil according to the same administration and dosage directions as for the treatment of dementia would suppress brain inflammation. This suggests that within the guaranteed safety range, donepezil could be applied for the treatment of brain inflammation and neurological complications in COVID-19 and that drug repositioning would allow it to be used in clinical practice at an early date. Therefore, its usefulness needs to be confirmed in clinical trials. As many aspects of their pathogenesis mechanisms are unknown and effective treatments have yet to be established, the results of the present study should not only contribute to the elucidation of pathologies, but also have high clinical value.

The present study also suggests the importance of promoting ZFP36 production via α7nAchRs in suppressing brain inflammation due to COVID-19. With this in mind, through the development of α7nAchR agonists, it may be possible to create more effective drugs for the treatment of brain inflammation in COVID-19 and prevention of long COVID. Also, by discovering an association of CAP and ZFP36 in the brain, we partly

elucidated the molecular mechanism of CAP and can expect this to provide clues for elucidating the mechanism of encephalopathy onset due to various causes including viruses and autoimmunity, as well as the development of treatments for them.

Limitations of the study

The effects of donepezil in the present research were obtained in an animal study. Therefore, in order to use it in the treatment of COVID-19 sequelae, its effects on patients will need to be confirmed through clinical trials or other methods.

STAR★METHODS

Detailed methods are provided in the online version of this paper and include the following:

- KEY RESOURCES TABLE
- RESOURCE AVAILABILITY
  - Lead contact
  - Materials availability
  - Data and code availability
- EXPERIMENTAL MODEL AND STUDY PARTICIPANT DETAILS
  - Animals
  - Cell lines
- METHOD DETAILS
  - Production of recombinant adenovirus vectors
  - Intracellular calcium assay
  - Nasal inoculation of adenovirus vectors
  - Drugs
  - Animal behavior tests
  - Real-time PCR
  - Immunohistochemistry
  - Measurement of brain acetylcholine levels
  - Induction of ZFP36 in cultured cells
- QUANTIFICATION AND STATISTICAL ANALYSIS

SUPPLEMENTAL INFORMATION

Supplemental information can be found online at https://doi.org/10.1016/j.isci.2023.106954.

ACKNOWLEDGMENTS

We thank Mr. Alexander Cox for editorial assistance with the manuscript. This research was supported by Japan Agency for Medical Research and Development (AMED) under Grant Number JP20fk0108541 and JP 21fk0108486.

AUTHOR CONTRIBUTIONS

N.O. and K.K. contributed to study design. N.O., K.S., A.I., N.K., and K.K. contributed to data collections or interpretation. K.K. coordinated all experiments.

DECLARATION OF INTERESTS

The authors declare no competing interests.

INCLUSION AND DIVERSITY

We support inclusive, diverse, and equitable conduct of research.

Received: October 20, 2022
Revised: February 21, 2023
Accepted: May 22, 2023
Published: May 24, 2023

REFERENCES

1. Chen, N., Zhou, M., Dong, X., Qu, J., Gong, F., Han, Y., Qiu, Y., Wang, J., Liu, Y., Wei, Y., et al. (2020). Epidemiological and clinical characteristics of 99 cases of 2019 novel coronavirus pneumonia in Wuhan, China: a descriptive study. Lancet *395*, 507–513. https://doi.org/10.1016/S0140-6736(20)30211-7.

2. Ariño, H., Heartshorne, R., Michael, B.D., Nicholson, T.R., Vincent, A., Pollak, T.A., and Vogrig, A. (2022). Neuroimmune disorders in COVID-19. J. Neurol. https://doi.org/10.1007/s00415-022-11050-w.

3. Solomon, T. (2021). Neurological infection with SARS-CoV-2 - the story so far. Nat. Rev. Neurol. *17*, 65–66. https://doi.org/10.1038/s41582-020-00453-w.

4. Guasp, M., Muñoz-Sánchez, G., Martínez-Hernández, E., Santana, D., Carbayo, Á., Naranjo, L., Bolós, U., Framil, M., Saiz, A., Balasa, M., et al. (2022). CSF biomarkers in COVID-19 associated encephalopathy and encephalitis predict long-term outcome. Front. Immunol. *13*, 866153. https://doi.org/10.3389/fimmu.2022.866153.

5. Vakili, K., Fathi, M., Hajiesmaeili, M., Salari, M., Saluja, D., Tafakhori, A., Sayehmiri, F., and Rezaei-Tavirani, M. (2021). Neurological symptoms, comorbidities, and complications of COVID-19: a literature review and meta-analysis of observational studies. Eur. Neurol. *84*, 307–324. https://doi.org/10.1159/000516258.

6. Ceban, F., Ling, S., Lui, L.M.W., Lee, Y., Gill, H., Teopiz, K.M., Rodrigues, N.B., Subramaniapillai, M., Di Vincenzo, J.D., Cao, B., et al. (2022). Fatigue and cognitive impairment in Post-COVID-19 Syndrome: a systematic review and meta-analysis. Brain Behav. Immun. *101*, 93–135. https://doi.org/10.1016/j.bbi.2021.12.020.

7. Schou, T.M., Joca, S., Wegener, G., and Bay-Richter, C. (2021). Psychiatric and neuropsychiatric sequelae of COVID-19 - a systematic review. Brain Behav. Immun. *97*, 328–348. https://doi.org/10.1016/j.bbi.2021.07.018.

8. Ibrahim, E.A.A., Isam Farah Hassan, R., Abbasher Hussien Mohamed Ahmed, K., Taha Salah, E., Eltahier Abdalla Omer, M., and Haroun, M.S. (2022). Neurological manifestations of COVID-19: a potential gate to the determinants of a poor prognosis. Brain Behav. *12*, e2587. https://doi.org/10.1002/brb3.2587.

9. Soriano, J.B., Murthy, S., Marshall, J.C., Relan, P., and Diaz, J.V.; WHO Clinical Case Definition Working Group on Post-COVID-19 Condition (2022). A clinical case definition of post-COVID-19 condition by a Delphi consensus. Lancet Infect. Dis. *22*, e102–e107. https://doi.org/10.1016/s1473-3099(21)00703-9.

10. Kaur, I., Behl, T., Sehgal, A., Singh, S., Sharma, N., Subramanian, V., Fuloria, S., Fuloria, N.K., Sekar, M., Dailah, H.G., et al. (2022). A motley of possible therapies of the COVID-19: reminiscing the origin of the pandemic. Environ. Sci. Pollut. Res. Int. *29*, 67685–67703. https://doi.org/10.1007/s11356-022-22345-w.

11. Behl, T., Shah, S., Kaur, I., Yadav, S., Kanwar, R., Seth, S., Wig, N., Sharma, K.K., and Yadav, H.N. (2021). Role of ACE 2 and vitamin D: the two players in global fight against COVID-19 pandemic. Ann. Natl. Acad. Med. Sci. *57*, 186–196.

12. Dal-Ré, R., Becker, S.L., Bottieau, E., and Holm, S. (2022). Availability of oral antivirals against SARS-CoV-2 infection and the requirement for an ethical prescribing approach. Lancet Infect. Dis. *22*, e231–e238. https://doi.org/10.1016/s1473-3099(22)00119-0.

13. Edwards, A.M., Baric, R.S., Saphire, E.O., and Ulmer, J.B. (2022). Stopping pandemics before they start: lessons learned from SARS-CoV-2. Science *375*, 1133–1139. https://doi.org/10.1126/science.abn1900.

14. Behl, T., Kaur, I., Aleya, L., Sehgal, A., Singh, S., Sharma, N., Bhatia, S., Al-Harrasi, A., and Bungau, S. (2022). CD147-spike protein interaction in COVID-19: Get the ball rolling with a novel receptor and therapeutic target. Sci. Total Environ. *808*, 152072. https://doi.org/10.1016/j.scitotenv.2021.152072.

15. Philips, R.L., Wang, Y., Cheon, H., Kanno, Y., Gadina, M., Sartorelli, V., Horvath, C.M., Darnell, J.E., Jr., Stark, G.R., and O'Shea, J.J. (2022). The JAK-STAT pathway at 30: much learned, much more to do. Cell *185*, 3857–3876. https://doi.org/10.1016/j.cell.2022.09.023.

16. Merad, M., Blish, C.A., Sallusto, F., and Iwasaki, A. (2022). The immunology and immunopathology of COVID-19. Science *375*, 1122–1127. https://doi.org/10.1126/science.abm8108.

17. Borah, P., Deb, P.K., Chandrasekaran, B., Goyal, M., Bansal, M., Hussain, S., Shinu, P., Venugopala, K.N., Al-Shar'i, N.A., Deka, S., and Singh, V. (2021). Neurological consequences of SARS-CoV-2 infection and concurrence of treatment-induced neuropsychiatric adverse events in COVID-19 patients: navigating the uncharted. Front. Mol. Biosci. *8*, 627723. https://doi.org/10.3389/fmolb.2021.627723.

18. Gorman, E.A., O'Kane, C.M., and McAuley, D.F. (2022). Acute respiratory distress syndrome in adults: diagnosis, outcomes, long-term sequelae, and management. Lancet *400*, 1157–1170. https://doi.org/10.1016/s0140-6736(22)01439-8.

19. Matschke, J., Lütgehetmann, M., Hagel, C., Sperhake, J.P., Schröder, A.S., Edler, C., Mushumba, H., Fitzek, A., Allweiss, L., Dandri, M., et al. (2020). Neuropathology of patients with COVID-19 in Germany: a post-mortem case series. Lancet Neurol. *19*, 919–929. https://doi.org/10.1016/s1474-4422(20)30308-2.

20. Yang, A.C., Kern, F., Losada, P.M., Agam, M.R., Maat, C.A., Schmartz, G.P., Fehlmann, T., Stein, J.A., Schaum, N., Lee, D.P., et al. (2021). Dysregulation of brain and choroid plexus cell types in severe COVID-19. Nature *595*, 565–571. https://doi.org/10.1038/s41586-021-03710-0.

21. Mukerji, S.S., and Solomon, I.H. (2021). What can we learn from brain autopsies in COVID-19? Neurosci. Lett. *742*, 135528. https://doi.org/10.1016/j.neulet.2020.135528.

22. McQuaid, C., Brady, M., and Deane, R. (2021). SARS-CoV-2: is there neuroinvasion? Fluids Barriers CNS *18*, 32. https://doi.org/10.1186/s12987-021-00267-y.

23. Fernández-Castañeda, A., Lu, P., Geraghty, A.C., Song, E., Lee, M.H., Wood, J., O'Dea, M.R., Dutton, S., Shamardani, K., Nwangwu, K., et al. (2022). Mild respiratory COVID can cause multi-lineage neural cell and myelin dysregulation. Cell *185*, 2452–2468. https://doi.org/10.1016/j.cell.2022.06.008.

24. Stein, S.R., Ramelli, S.C., Grazioli, A., Chung, J.Y., Singh, M., Yinda, C.K., Winkler, C.W., Sun, J., Dickey, J.M., Ylaya, K., et al. (2022). SARS-CoV-2 infection and persistence in the human body and brain at autopsy. Nature *612*, 758–763. https://doi.org/10.1038/s41586-022-05542-y.

25. Klingenstein, M., Klingenstein, S., Neckel, P.H., Mack, A.F., Wagner, A.P., Kleger, A., Liebau, S., and Milazzo, A. (2020). Evidence of SARS-CoV2 entry protein ACE2 in the human nose and olfactory bulb. Cells Tissues Organs *209*, 155–164. https://doi.org/10.1159/000513040.

26. Brann, D.H., Tsukahara, T., Weinreb, C., Lipovsek, M., Van den Berge, K., Gong, B., Chance, R., Macaulay, I.C., Chou, H.J., Fletcher, R.B., et al. (2020). Non-neuronal expression of SARS-CoV-2 entry genes in the olfactory system suggests mechanisms underlying COVID-19-associated anosmia. Sci. Adv. *6*, eabc5801. https://doi.org/10.1126/sciadv.abc5801.

27. Kandemirli, S.G., Altundag, A., Yildirim, D., Tekcan Sanli, D.E., and Saatci, O. (2021). Olfactory bulb MRI and paranasal sinus CT findings in persistent COVID-19 anosmia. Acad. Radiol. *28*, 28–35. https://doi.org/10.1016/j.acra.2020.10.006.

28. Altunisik, E., Baykan, A.H., Sahin, S., Aydin, E., and Erturk, S.M. (2021). Quantitative analysis of the olfactory system in COVID-19: an MR imaging study. AJNR. Am. J. Neuroradiol. *42*, 2207–2214. https://doi.org/10.3174/ajnr.A7278.

29. Tan, C.J.W., Tan, B.K.J., Tan, X.Y., Liu, H.T., Teo, C.B., See, A., Xu, S., Toh, S.T., Kheok, S.W., Charn, T.C., and Teo, N.W.Y. (2022). Neuroradiological basis of COVID-19 olfactory dysfunction: a systematic review and meta-analysis. Laryngoscope *132*, 1260–1274. https://doi.org/10.1002/lary.30078.

30. Rinwa, P., and Kumar, A. (2013). Quercetin suppress microglial neuroinflammatory response and induce antidepressant-like effect in olfactory bulbectomized rats. Neuroscience *255*, 86–98. https://doi.org/10.1016/j.neuroscience.2013.09.044.

31. Almeida, R.F.d., Ganzella, M., Machado, D.G., Loureiro, S.O., Leffa, D., Quincozes-Santos, A., Pettenuzzo, L.F., Duarte, M.M., Duarte, T., and Souza, D.O. (2017). Olfactory bulbectomy in mice triggers transient and long-lasting behavioral impairments and biochemical hippocampal disturbances. Prog. Neuro-Psychopharmacol. Biol. Psychiatry *76*, 1–11. https://doi.org/10.1016/j.pnpbp.2017.02.013.

32. Bansal, Y., Singh, R., Saroj, P., Sodhi, R.K., and Kuhad, A. (2018). Naringenin protects against oxido-inflammatory aberrations and altered tryptophan metabolism in olfactory bulbectomized-mice model of depression. Toxicol. Appl. Pharmacol. *355*, 257–268. https://doi.org/10.1016/j.taap.2018.07.010.

33. Thyssen, A., Hirnet, D., Wolburg, H., Schmalzing, G., Deitmer, J.W., and Lohr, C. (2010). Ectopic vesicular neurotransmitter release along sensory axons mediates neurovascular coupling via glial calcium signaling. Proc. Natl. Acad. Sci. USA *107*, 15258–15263. https://doi.org/10.1073/pnas.1003501107.

34. Kobayashi, N., Oka, N., Takahashi, M., Shimada, K., Ishii, A., Tatebayashi, Y., Shigeta, M., Yanagisawa, H., and Kondo, K. (2020). Human herpesvirus 6B greatly increases risk of depression by activating hypothalamic-pituitary -adrenal Axis during latent phase of infection. iScience *23*, 101187. https://doi.org/10.1016/j.isci.2020.101187.

35. Braga, L., Ali, H., Secco, I., Chiavacci, E., Neves, G., Goldhill, D., Penn, R., Jimenez-Guardeño, J.M., Ortega-Prieto, A.M., Bussani, R., et al. (2021). Drugs that inhibit TMEM16 proteins block SARS-CoV-2 spike-induced syncytia. Nature *594*, 88–93. https://doi.org/10.1038/s41586-021-03491-6.

36. Ramaker, M.J., and Dulawa, S.C. (2017). Identifying fast-onset antidepressants using rodent models. Mol. Psychiatr. *22*, 656–665. https://doi.org/10.1038/mp.2017.36.

37. Su, K.Y., Yu, C.Y., Chen, Y.W., Huang, Y.T., Chen, C.T., Wu, H.F., and Chen, Y.L.S. (2014). Rutin, a flavonoid and principal component of saussurea involucrata, attenuates physical fatigue in a forced swimming mouse model. Int. J. Med. Sci. *11*, 528–537. https://doi.org/10.7150/ijms.8220.

38. Can, A., Dao, D.T., Terrillion, C.E., Piantadosi, S.C., Bhat, S., and Gould, T.D. (2011). The tail suspension test. J. Vis. Exp. e3769. https://doi.org/10.3791/3769.

39. Schroeder, J.T., and Bieneman, A.P. (2022). The S1 subunit of the SARS-CoV-2 spike protein activates human monocytes to produce cytokines linked to COVID-19: relevance to galectin-3. Front. Immunol. *13*, 831763. https://doi.org/10.3389/fimmu.2022.831763.

40. Fisman, D.N., and Tuite, A.R. (2021). Evaluation of the relative virulence of novel SARS-CoV-2 variants: a retrospective cohort study in Ontario, Canada. CMAJ (Can. Med. Assoc. J.) *193*. E1619–e1625. https://doi.org/10.1503/cmaj.211248.

41. Venkatraja, B., Srilakshminarayana, G., and Krishna Kumar, B. (2021). The dominance of severe acute respiratory syndrome coronavirus 2 B.1.617 and its sublineages and associations with mortality during the COVID-19 pandemic in India between 2020 and 2021. Am. J. Trop. Med. Hyg. *106*, 142–149. https://doi.org/10.4269/ajtmh.21-0812.

42. Tracey, K.J. (2009). Reflex control of immunity. Nat. Rev. Immunol. *9*, 418–428. https://doi.org/10.1038/nri2566.

43. Hoover, D.B. (2017). Cholinergic modulation of the immune system presents new approaches for treating inflammation. Pharmacol. Ther. *179*, 1–16. https://doi.org/10.1016/j.pharmthera.2017.05.002.

44. Piovesana, R., Salazar Intriago, M.S., Dini, L., and Tata, A.M. (2021). Cholinergic modulation of neuroinflammation: focus on α7 nicotinic receptor. Int. J. Mol. Sci. *22*, 4912. https://doi.org/10.3390/ijms22094912.

45. Reardon, C. (2016). Neuro-immune interactions in the cholinergic anti-inflammatory reflex. Immunol. Lett. *178*, 92–96. https://doi.org/10.1016/j.imlet.2016.08.006.

46. Makita, S., Takatori, H., and Nakajima, H. (2021). Post-transcriptional regulation of immune responses and inflammatory diseases by RNA-binding ZFP36 family proteins. Front. Immunol. *12*, 711633. https://doi.org/10.3389/fimmu.2021.711633.

47. Kalashnyk, O., Lykhmus, O., Oliinyk, O., Komisarenko, S., and Skok, M. (2014). α7 Nicotinic acetylcholine receptor-specific antibody stimulates interleukin-6 production in human astrocytes through p38-dependent pathway. Int. Immunopharm. *23*, 475–479. https://doi.org/10.1016/j.intimp.2014.09.022.

48. Kuwajima, T., Nishimura, I., and Yoshikawa, K. (2006). Necdin promotes GABAergic neuron differentiation in cooperation with Dlx homeodomain proteins. J. Neurosci. *26*, 5383–5392. https://doi.org/10.1523/jneurosci.1262-06.2006.

49. Kalinowski, D., Bogus-Nowakowska, K., Kozłowska, A., and Równiak, M. (2022). Expression of calbindin, a marker of gamma-aminobutyric acid neurons, is reduced in the amygdala of oestrogen receptor β-deficient female mice. J. Clin. Med. *11*, 1760. https://doi.org/10.3390/jcm11071760.

50. Birks, J.S., and Harvey, R.J. (2018). Donepezil for dementia due to Alzheimer's disease. Cochrane Database Syst. Rev. *6*, Cd001190. https://doi.org/10.1002/14651858.CD001190.pub3.

51. Ricciardi, L., Col, J.D., Casolari, P., Memoli, D., Conti, V., Vatrella, A., Vonakis, B.M., Papi, A., Caramori, G., and Stellato, C. (2018). Differential expression of RNA-binding proteins in bronchial epithelium of stable COPD patients. Int. J. Chronic Obstr. Pulm. Dis. *13*, 3173–3190. https://doi.org/10.2147/copd.S166284.

52. Mahar, I., Bambico, F.R., Mechawar, N., and Nobrega, J.N. (2014). Stress, serotonin, and hippocampal neurogenesis in relation to depression and antidepressant effects. Neurosci. Biobehav. Rev. *38*, 173–192. https://doi.org/10.1016/j.neubiorev.2013.11.009.

53. Gonçalves, J.T., Schafer, S.T., and Gage, F.H. (2016). Adult neurogenesis in the Hippocampus: from stem cells to behavior. Cell *167*, 897–914. https://doi.org/10.1016/j.cell.2016.10.021.

54. Ho, C.Y., Salimian, M., Hegert, J., O'Brien, J., Choi, S.G., Ames, H., Morris, M., Papadimitriou, J.C., Mininni, J., Niehaus, P., et al. (2022). Postmortem assessment of olfactory tissue degeneration and microvasculopathy in patients with COVID-19. JAMA Neurol. *79*, 544–553. https://doi.org/10.1001/jamaneurol.2022.0154.

55. Gonzalez-Rubio, J., Navarro-Lopez, C., Lopez-Najera, E., Lopez-Najera, A., Jimenez-Diaz, L., Navarro-Lopez, J.D., and Najera, A. (2020). Cytokine release syndrome (CRS) and nicotine in COVID-19 patients: trying to calm the storm. Front. Immunol. *11*, 1359. https://doi.org/10.3389/fimmu.2020.01359.

56. Mehranfard, D., and Speth, R.C. (2022). Cholinergic anti-inflammatory pathway and COVID-19. Bioimpacts *12*, 171–174. https://doi.org/10.34172/bi.2022.23980.

57. Courties, A., Boussier, J., Hadjadj, J., Yatim, N., Barnabei, L., Péré, H., Veyer, D., Kernéis, S., Carlier, N., Pène, F., et al. (2021). Regulation of the acetylcholine/α7nAChR anti-inflammatory pathway in COVID-19 patients. Sci. Rep. *11*, 11886. https://doi.org/10.1038/s41598-021-91417-7.

58. Han, F., Shioda, N., Moriguchi, S., Qin, Z.H., and Fukunaga, K. (2008). The vanadium (IV) compound rescues septo-hippocampal cholinergic neurons from neurodegeneration in olfactory bulbectomized mice. Neuroscience *151*, 671–679. https://doi.org/10.1016/j.neuroscience.2007.11.011.

59. Ferrer, I. (1999). Neurons and their dendrites in frontotemporal dementia. Dement. Geriatr. Cogn. Disord *10* (*Suppl 1*), 55–60. https://doi.org/10.1159/000051214.

60. Fujiwara, N., and Cave, J.W. (2016). Partial conservation between mice and humans in olfactory bulb interneuron transcription factor codes. Front. Neurosci. *10*, 337. https://doi.org/10.3389/fnins.2016.00337.

61. Versace, V., Sebastianelli, L., Ferrazzoli, D., Romanello, R., Ortelli, P., Saltuari, L., D'Acunto, A., Porrazzini, F., Ajello, V., Oliviero, A., et al. (2021). Intracortical GABAergic dysfunction in patients with fatigue and dysexecutive syndrome after COVID-19. Clin. Neurophysiol. *132*, 1138–1143. https://doi.org/10.1016/j.clinph.2021.03.001.

62. Ortelli, P., Ferrazzoli, D., Sebastianelli, L., Maestri, R., Dezi, S., Spampinato, D., Saltuari, L., Alibardi, A., Engl, M., Kofler, M., et al. (2022). Altered motor cortex physiology and dysexecutive syndrome in patients with fatigue and cognitive difficulties after mild COVID-19. Eur. J. Neurol. *29*, 1652–1662. https://doi.org/10.1111/ene.15278.

63. Piras, I.S., Huentelman, M.J., Walker, J.E., Arce, R., Glass, M.J., Vargas, D., Sue, L.I., Intorcia, A.J., Nelson, C.M., Suszczewicz, K.E., et al. (2021). Olfactory bulb and amygdala gene expression changes in subjects dying with COVID-19. Preprint at medRxiv. https://doi.org/10.1101/2021.09.12.21263291.

64. Guedj, E., Million, M., Dudouet, P., Tissot-Dupont, H., Bregeon, F., Cammilleri, S., and Raoult, D. (2021). (18 F-FDG brain PET hypometabolism in post-SARS-CoV-2 infection: substrate for persistent/delayed disorders? Eur. J. Nucl. Med. Mol. Imag. *48*, 592–595. https://doi.org/10.1007/s00259-020-04973-x.

65. Campabadal, A., Oltra, J., Junqué, C., Guillen, N., Botí, M.Á., Sala-Llonch, R., Monté-Rubio, G.C., Lledó, G., Bargalló, N., Rami, L., et al. (2022). Structural brain changes in post-acute COVID-19 patients with persistent olfactory dysfunction. Ann. Clin. Transl. Neurol. *10*, 195–203. https://doi.org/10.1002/acn3.51710.

66. Besteher, B., Machnik, M., Troll, M., Toepffer, A., Zerekidze, A., Rocktäschel, T., Heller, C., Kikinis, Z., Brodoehl, S., Finke, K., et al. (2022). Larger gray matter volumes in neuropsychiatric long-COVID syndrome. Psychiatr. Res. *317*, 114836. https://doi.org/10.1016/j.psychres.2022.114836.

67. Martini, A.L., Carli, G., Kiferle, L., Piersanti, P., Palumbo, P., Morbelli, S., Calcagni, M.L., Perani, D., and Sestini, S. (2022). Time-dependent recovery of brain hypometabolism in neuro-COVID-19 patients. Eur. J. Nucl. Med. Mol. Imag. *50*, 90–102. https://doi.org/10.1007/s00259-022-05942-2.

68. Shin, C.Y., Kim, H.S., Cha, K.H., Won, D.H., Lee, J.Y., Jang, S.W., and Sohn, U.D. (2018). The effects of donepezil, an acetylcholinesterase inhibitor, on impaired learning and memory in rodents. Biomol. Ther. (Seoul) *26*, 274–281. https://doi.org/10.4062/biomolther.2017.189.

STAR★METHODS

KEY RESOURCES TABLE

REAGENT or RESOURCE	SOURCE	IDENTIFIER
Antibodies		
Rabbit polyclonal anti-active Caspase 3	Abcam	Cat# ab13847; RRID: AB_443014
Rabbit polyclonal anti-Doublecortin	Abcam	Cat# ab18723; RRID: AB_732011
Rabbit polyclonal anti- Choline Acetyltransferase	Abcam	Cat# ab178850; RRID: AB_2721842
Goat anti-Rabbit IgG (H + L) Highly Cross-Adsorbed Secondary Antibody, Alexa Fluor 488	ThermoFisher	Cat# A-11034; RRID: AB_2576217
Bacterial and virus strains		
Vector-Ad	TaKaRa Bio	Cat# 6170
S1-Ad	This paper	N/A
Chemicals, peptides, and recombinant proteins		
Donepezil Hydrochloride	FUJIFILM Wako Chemicals	Cat# 041-32323
PNU 282987	FUJIFILM Wako Chemicals	Cat# 167-26363
Lipopolysaccharides from *Escherichia coli* O111:B4	Merk	Cat# L2630-100 MG
Image-iT FX Signal Enhancer	Invitrogen	Cat# I36933
Can Get Signal Immunostain Solution A	TOYOBO	Cat# NKB-501
ProLong Diamond Antifade Mountant with DAPI	ThermoFisher	Cat# P36962
Premix Ex Taq (Perfect Real Time)	TaKaRa Bio	Cat# RR039A
Critical commercial assays		
Adenovirus Dual Expression Kit	TaKaRa Bio	Cat# 6170
ProFection Mammalian Transfection System	Promega	Cat# E1200
Calcium Kit II – Fluo 4	Dojindo	Cat# CS32
Adeno-X Virus Purification kit	Takara Bio	Cat# 631532
Adeno-X Rapid Titer kit	Takara Bio	Cat# 632250
RNeasy Mini QIAcube Kit	QIAGEN	Cat# 74116
PrimeScript RT Reagent Kit	Takara Bio	Cat# RR037A
Choline/Acetylcholine Assay Kit	Abcam	Cat# ab65345
Deposited data		
Original Data	Mendeley Data	https://doi.org/10.17632/ch52rydwjh.1
Experimental models: Cell lines		
Mouse: 3T3 (NIH/3T3)	RIKEN BRC	RCB2767
Human: A549	RIKEN BRC	RCB0098
Human: U373 (U-373 MG)	ATCC	HBT-17
Experimental models: Organisms/strains		
C57BL/6NCrSlc	Japan SLC,Inc.	N/A
Oligonucleotides		
SARS-CoV-2_S1 qPCR F: CTGACGGAGAGCAATAAGAAGTTTC R: CCAGGATTTCCAGTGTCTGAGG P: FAM- CCATTCCAGCAGTTCGGCAG AGACATTG -TAMRA	This paper	N/A
Mm_IL-6 qPCR	ThermoFisher	Mm00446190_m1

(*Continued on next page*)

Continued

REAGENT or RESOURCE	SOURCE	IDENTIFIER
Mm_IL-1β qPCR	ThermoFisher	Mm00434228_m1
Mm_TNFα qPCR	ThermoFisher	Mm00443258_m1
Mm_CCL2 qPCR	ThermoFisher	Mm00441242_m1
Mm_Zfp36 qPCR	ThermoFisher	Mm00457144_m1
Mm_Calbindin qPCR	ThermoFisher	Mm00486647_m1
Mm_GFAP qPCR	ThermoFisher	Mm01253033_m1
Mm_Nestin qPCR	ThermoFisher	Mm00450205_m1
Mm_IL-17a qPCR	ThermoFisher	Mm00439618_m1
Mm_Sox2 qPCR	ThermoFisher	Mm03053810_s1
Mm_Mcm2 qPCR	ThermoFisher	Mm00484815_m1
Mm_DCX qPCR	ThermoFisher	Mm00438400_m1
Mm_Calretinin qPCR	ThermoFisher	Mm00801461_m1
Mm_HuR qPCR	ThermoFisher	Mm00516011_m1
Mm_Roquin qPCR	ThermoFisher	Mm01284492_m1
Mm_KHSRP qPCR	ThermoFisher	Mm01232838_g1
Mm_Regnase-1 qPCR	ThermoFisher	Mm00462535_g1
Mm_AUF1 qPCR	ThermoFisher	Mm01201314_m1
18s rRNA	ThermoFisher	Hs99999901_s1
Recombinant DNA		
pFlag-CMV-5b	Sigma Aldrich	Cat# E3762
SARS-CoV-2 S1 (Wu)/pFlag-CMV-5b	This paper	N/A
SARS-CoV-2 S1 (α)/pFlag-CMV-5b	This paper	N/A
SARS-CoV-2 S1 (δ)/pFlag-CMV-5b	This paper	N/A
SARS-CoV-2 NTD/pFlag-CMV-5b	This paper	N/A
SARS-CoV-2 Spike/pFlag-CMV-5b	This paper	N/A
Software and algorithms		
ImageJ	NIH	https://imagej.nih.gov/ij/
Sequence Detection Software version 1.4	Thermo Fisher	N/A
Prism 8	GraphPad	N/A
BellCurve for Excel	Social Survey Research Information Co., Ltd	https://bellcurve.jp/ex/
TailSuspScan	CleverSys Inc	N/A
TopScan	CleverSys Inc	N/A
ArrayScan XTI instrument	Thermo Fisher	N/A

RESOURCE AVAILABILITY

Lead contact

Further information and requests for resources and reagents should be directed to and will be fulfilled by the Lead Contact, Kazuhiro Kondo (kkondo@jikei.ac.jp).

Materials availability

All unique reagents generated in this study are available from the lead contact with a completed Materials Transfer Agreement.

Data and code availability

- The data included in this manuscript have been deposited at Mendeley Data and publicly available as of the date of publication. The DOI is listed in the key resources table.

- This paper does not report original code.
- Any additional information required to reanalyze the data reported in this paper is available from the lead contact upon request.

EXPERIMENTAL MODEL AND STUDY PARTICIPANT DETAILS

Animals

Male 8-week-old C57BL/6NCrSlc mice obtained from Sankyo laboratories were used for all experiments. All mice were housed under standard conditions (12-h light–dark cycle [lights-on at 8:00 a.m.] at 24 ± 1°C) with food and water provided *ad libitum*. All animal experiments were performed in accordance with animal experiment regulations and approved by the Animal Care and Use Committee of the Jikei University School of Medicine.

Cell lines

The mouse fibroblast-like cell line 3T3, human lung epithelial cell line A549, human astrocytoma cell lines U373 and human embryonic kidney cell line HEK293A were cultured in Dulbecco's modified Eagle's medium (DMEM) containing 10% FBS. These cells were incubated at 37°C in a humidified 5% CO2 atmosphere. Sex and age at sampling for the cells were as follows: 3T3, male embryo; A549, male 58Y; U373, male 75Y; HEK293A, female fetus.

METHOD DETAILS

Production of recombinant adenovirus vectors

The recombinant adenovirus was produced using an Adenovirus Dual Expression Kit (Takara Bio) in accordance with the manufacturer's protocol. The SARS-CoV-2 genes were cloned into an adenovirus cosmid vector (pAxCAwtit2) using standard methods (SARS-CoV-2 genes/pAxCAwtit2). HEK293A cells were transfected with the SARS-CoV-2 genes/pAxCAwtit2 cosmid and a cosmid that did not contain the target gene (pAxcwit2). The recombinant adenovirus was prepared in HEK293A cells and purified with an Adeno-X Virus Purification kit (Takara Bio). The purified virus titer was determined using an Adeno-X Rapid Titer kit (Takara Bio).

Intracellular calcium assay

3T3 cells or A549 cells were cultured on a 96-well plate and transient overexpression of each protein - S1 (Wu, α and δ) - was achieved for 24 h using ProFection Mammalian Transfection System (Promega) or adenovirus infection. Subsequently, cells were induced to take up Fluo 4-AM using Calcium Kit II-Fluo 4 (Dojindo) and then the fluorescence intensity in individual cells was measured using an ArrayScan XTI instrument (Thermo Fisher).

Nasal inoculation of adenovirus vectors

For the nasal inoculation of adenovirus vectors, 8-week-old male C57BL/6 mice were anesthetized with isoflurane. Recombinant adenoviruses were diluted in sterile water (not in isotonic buffer). A drop (25 μL) of S1-Ad or Vector-Ad solution containing the virus at a titer of 1×10^9 infectious units (ifu)/mL was placed at the entrance of the nasal cavity of the mouse. The solution entered the cavity through spontaneous respiration.

Drugs

The cholinesterase inhibitor donepezil (FUJIFILM Wako) was administered via the drinking water (40 mg/L, 4 mg/kg/day) from the day of intranasal inoculation. For oral administration, donepezil was diluted in saline and administered to mice by feeding tube at 0, 1 and 2 mg/kg. The α7nAChR agonist PNU282987 (FUJIFILM Wako) was diluted in saline and administered intracerebroventricularly at 400 nmol/mouse. Lipopolysaccharide (LPS) from *Escherichia coli* O111:B4 (Merck) was diluted in saline and administered intraperitoneally to S1 mice at 5 mg/kg. The brain and olfactory bulb were removed 15 and 30 min after administration, respectively, and used for gene expression analysis. For all oral, intracerebroventricular and intraperitoneal administrations, control mice received the solvent saline.

Animal behavior tests

Seven days after the inoculation of S1-Ad or Vector-Ad, a tail suspension test (TST) and a weight-loaded forced swim test (WFST) were performed to assess depression- and fatigue-like behavior. In the TST, the period of immobility during 10 min was analyzed by TailSuspScan software (CleverSys Inc). In the WFST, a weight equivalent to 10% of body weight was attached to the root of the mouse tail, the time taken for the mouse's nose to be below the surface of the water for 10 s was measured by TopScan software (CleverSys Inc). At 24 h, after these behavior tests, the mice were euthanized for real-time PCR and immunohistochemical staining.

Real-time PCR

Total RNA was purified from animal tissues using the RNeasy Mini QIAcube Kit (Qiagen). cDNA was synthesized from total RNA with a PrimeScript RT Reagent Kit (Takara Bio). mRNA amounts were quantified with Premix Ex Taq (Perfect Real Time) (Takara Bio), and the Applied Biosystems 7300 Real-Time PCR system (Thermo Fisher). The thermal profile was 95°C for 30 s, followed by 45 cycles of 95°C for 5 s and 60°C for 31 s. Data analysis was performed with Sequence Detection Software version 1.4 (Thermo Fisher). Mouse IL-6, mouse IL-1β, mouse TNFα, mouse CCL-2, mouse ZFP36, mouse Calbindin, mouse GFAP, mouse Nestin, mouse Sox2, mouse Mcm2, mouse DCX, mouse Calretinin, mouse HuR, mouse Roquin, mouse KHSRP, mouse Regnase-1, mouse AUF1, human 18S and SARS-CoV-2 S1 were measured using the primers and probes described in the key resources table.

Immunohistochemistry

For the staining of tissues, mice were sacrificed and transcardially perfused with saline, followed by 10% neutral buffered formalin (pH 7.4). Formalin-fixed tissues were then embedded in paraffin and sectioned. For immunofluorescence staining, paraffin-embedded sections were deparaffinized, and blocking was performed in Image-iT FX Signal Enhancer (Life Technologies) for 30 min. Primary antibodies were obtained from Abcam (active caspase-3, doublecortin and Choline Acetyltransferase). Secondary antibodies were obtained from Thermo (Alexa Fluor 488 Goat Anti-rabbit IgG (H + L)). The antibodies were diluted with Can Get Signal Immunostain Solution A (TOYOBO). After the samples had been mounted on a slide with a cover glass, they were observed under a Keyence BZ-9000 fluorescence microscope.

Measurement of brain acetylcholine levels

Seven days after the inoculation of S1-Ad or Vector-Ad, mice were sacrificed and their brains immediately harvested. The amount of acetylcholine in the brain was measured by the Choline/Acetylcholine Assay Kit (abcam). Fluorescence was measured by TriStar LB941 (Berthold).

Induction of ZFP36 in cultured cells

U373 cells were cultured on a 6-well plate and stimulated with 10 μM PNU282987. After culturing U373 cells in the presence of 10 μg/mL LPS (Merck) for 48 h, they were stimulated with 10 μM PNU282987.Cells were recovered 2h after stimulation followed by RNA purification and cDNA synthesis by the methods mentioned above and then expression of anti-inflammatory factors was analyzed by RT-qPCR. Human TNFα, Human ZFP36 and human 18S were measured using the primers and probes described in the key resources table.

QUANTIFICATION AND STATISTICAL ANALYSIS

The Shapiro-Wilk normality test was performed to assess the normality of distributions. To compare two different groups, the Mann-Whitney U-test was used as the nonparametric test. To compare multiple groups, the Kruskal-Wallis test, and then Dunn's post hoc test, were used as nonparametric tests. Red horizontal lines are medians. $p < 0.05$ was considered significant. Spearman's rank correlation coefficients were used to determine correlations between variables. Statistical analyses were performed with Prism 8 (GraphPad) and BellCurve for Excel (Social Survey Research Information Co., Ltd.).